

Hierarchical Graph Generation with K^2 -trees

Yunhui Jang
POSTECH

uni5510@postech.ac.kr

Dongwoo Kim
POSTECH

dongwookim@postech.ac.kr

Sungsoo Ahn
POSTECH

sungsoo.ahn@postech.ac.kr

Abstract

Generating graphs from a target distribution is a significant challenge across many domains, including drug discovery and social network analysis. In this work, we introduce a novel graph generation method leveraging K^2 -tree representation which was originally designed for lossless graph compression. Our motivation stems from the ability of the K^2 -tree to enable compact generation while concurrently capturing the inherent hierarchical structure of a graph. In addition, we make further contributions by (1) presenting a sequential K^2 -tree representation that incorporates pruning, flattening, and tokenization processes and (2) introducing a Transformer-based architecture designed to generate the sequence by incorporating a specialized tree positional encoding scheme. Finally, we extensively evaluate our algorithm on four general and two molecular graph datasets to confirm its superiority for graph generation.

1 Introduction

Generating graph-structured data is a challenging problem in numerous fields, such as molecular design [1; 2], social network analysis [3], and public health [4]. Recently, deep generative models have demonstrated significant potential in addressing this challenge [2; 5; 6; 7; 8; 9]. In contrast to the classic random graph models [10; 11], these methods leverage powerful deep generative paradigms, e.g., variational autoencoders [5], normalizing flows [6], and diffusion models [8].

The deep graph generative models can be categorized into three types by their graph representation. First, a common approach is to directly generate the adjacency matrix of the graph [5; 6; 7; 2]. Alternatively, some models generate a string representation of the graph, extracted from applying depth-first tree traversal [12; 13; 14; 15]. Finally, there exist works that formulate graphs as a composition of motifs, i.e., frequently appearing subgraphs [16; 17]. We describe the representations on the left of Figure 1.

Although there is no consensus on the best graph representation, two factors drive their development. First is the need for compactness to reduce the complexity of graph generation and simplify the search space over graphs. For example, to generate a graph with N vertices and M edges, the adjacency matrix requires specifying $O(N^2)$ elements. In contrast, the string representation typically requires specifying $O(N + M)$ elements, leveraging the graph sparsity [12; 13; 15]. Motif representations also save space by representing frequently appearing subgraphs by tokens [16; 17].

The second factor driving the development of new graph representations is the presence of a hierarchy in graphs. For instance, community graphs possess underlying clusters, molecular graphs consist of distinct chemical fragments, and grid graphs exhibit a repetitive coarse-graining structure. In this context, motif representations [16; 17] address the presence of a hierarchy in molecular graphs;

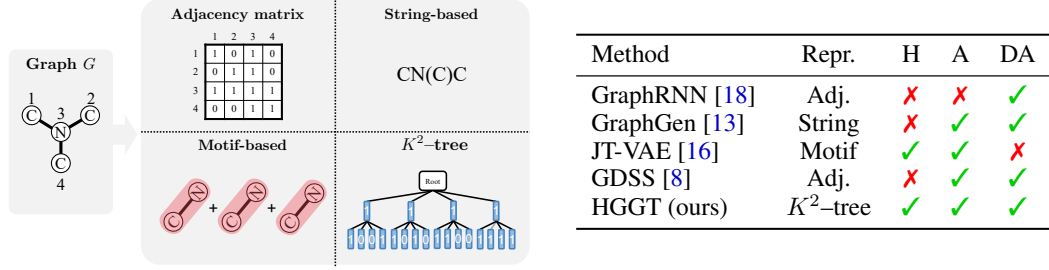


Figure 1: **(Left) Various representations used for graph generation. (Right) Comparing graph generative methods in terms of used graph representation.** The comparison is made with respect to a method being domain-agnostic (DA), hierarchical (H), and able to handle attributed graphs (A).

however, they are currently limited to expressing hierarchy for a fixed vocabulary of motifs in a specific domain and cannot be generalized to capture the hierarchical structure of general graphs.

Contribution. In this paper, we propose a novel graph generation framework, coined **Hierarchical Graph Generation with K^2 -Tree (HGGT)**, which is compact, hierarchical, able to represent attributed graphs, and does not require domain-specific rules. The right-side table of Figure 1 further emphasizes the benefits of our method. Since the K^2 -tree was originally proposed for lossless graph compression, we adopt it to graph generation by processing it into a sequence and developing an autoregressive model to generate the sequence.

Specifically, we aim to train an autoregressive model for the K^2 -tree where a sequential representation for the generative procedure is necessary. To this end, we design a sequential representation that is even more compact than the K^2 -tree as it minimizes the number of decisions required for the autoregressive model. In particular, we propose a two-stage procedure where (1) we prune the K^2 -tree to remove redundancy arising from the symmetric adjacency matrix for undirected graphs and (2) subsequently flatten and tokenize the K^2 -tree into a sequence to minimize the number of decisions required for the graph generation.

We employ the Transformer architecture [19] to generate a K^2 -tree representation of a graph. To better incorporate the positional information of each tree-node, we design a new positional encoding scheme specialized to the K^2 -tree structure. Specifically, we represent the positional information of a tree-node by its pathway from the root node; this is an informative encoding since one can reconstruct the full K^2 -tree given just the positional information.

To validate the effectiveness of our algorithm, we test our method on popular graph generation benchmarks across six graph datasets: Community, Enzymes [20], Grid, Planar, ZINC [21], and QM9 [22]. Our empirical results confirm that HGGT significantly outperformed existing graph generation methods on five out of six benchmarks, verifying the capability of our approach for high-quality graph generation across diverse applications.

To summarize, our key contributions are as follows:

- We propose a new graph generative model based on adopting the K^2 -tree as a compact, hierarchical, and domain-agnostic representation of graphs.
- We introduce a novel, compact sequential K^2 -tree representation obtained from pruning, flattening, and tokenizing the K^2 -tree.
- We propose an autoregressive model to generate the sequential K^2 -tree representation using Transformer architecture with a specialized positional encoding scheme.
- We validate the efficacy of our framework by demonstrating state-of-the-art graph generation performance on five out of six graph generation benchmarks.

2 Related Work

Adjacency matrix-based graph generation. The choice of graph representation is a crucial aspect of graph generation, as it can significantly impact the efficiency and expressiveness of the generative model. The most widely used representation is the adjacency matrix, which explicitly encodes the

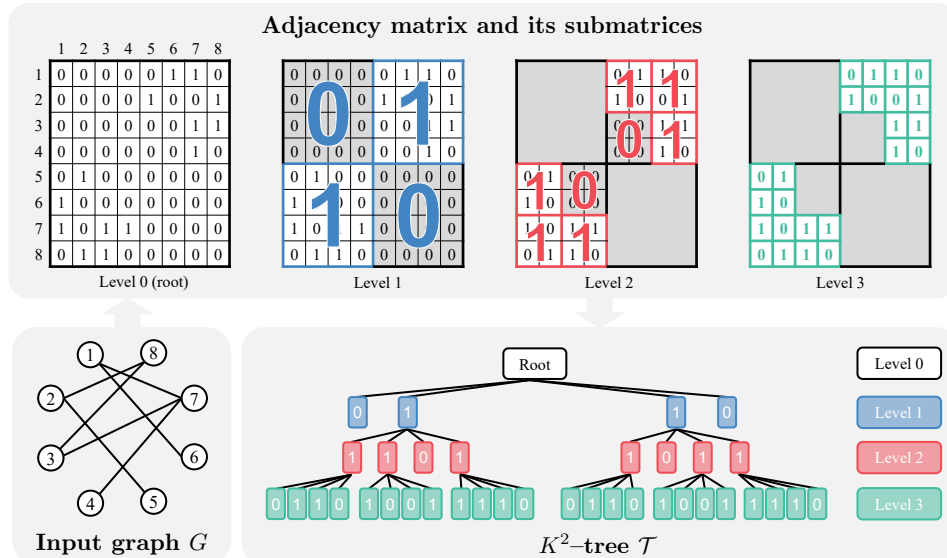


Figure 2: K^2 -tree with $K = 2$. The K^2 -tree describes the hierarchy of the adjacency matrix iteratively being partitioned to $K \times K$ submatrices. It is compact due to summarizing any zero-filled submatrix with size larger than 1×1 (shaded in grey) by a non-leaf node u with label $x_u = 0$.

simple pairwise relationship between nodes [5; 8; 9; 18; 23; 24; 25; 26]. However, these methods suffer from high complexity in generating the adjacency matrix, especially for large graphs.

String-based graph generation. Researchers have developed string-based representations [12; 14; 15]. In particular, for the molecular graph generation, Segler et al. [15] considered generating the SMILES representation [27]. Since the SMILES representation may be invalid, Krenn et al. [14] designed a robust string-based representation of molecules. Finally, Ahn et al. [12] designed a new representation to exploit the tree-like structure of molecules. For general graph generation, Goyal et al. [13] designed a string representation using a graph canonicalization algorithm.

Motif-based graph generation. Researchers have investigated motif-based graph representations [16; 17; 28] that capture hierarchical graph structures with lower computational costs. Specifically, Jin et al. [16; 17] considered extracting common fragments from data. Yang et al. [28] considered chemically reasonable fragments defined by domain experts. Finally, Guo et al. [29] considered learning motif-based grammar by running a reinforcement learning algorithm on the dataset. However, these methods rely on domain-specific knowledge to define or extract the motifs from data.

Lossless graph compression. Similar to the representations used for graph generation, lossless graph compression [30] aims to reduce the size and complexity of graphs while preserving their underlying structures. Specifically, several works [31; 32] have introduced hierarchical graph compression methods that efficiently compress graphs by leveraging their hierarchical structure. In addition, Bouritsas et al. [33] derived the compressed representation using a learning-based objective.

3 Preliminary: K^2 -tree Representation of a Graph

In this section, we introduce the K^2 -tree as a hierarchical and compact representation of graphs, as originally proposed for graph compression [31]. In essence, the K^2 -tree is a K^2 -ary ordered tree that recursively partitions the adjacency matrix into $K \times K$ submatrices.¹ Its key idea is to summarize the submatrices filled only with zeros with a single tree-node, exploiting sparsity of the adjacency matrix. The representation is hierarchical, as it associates each parent and child node pair with a matrix and its corresponding submatrix, respectively. An illustration of the K^2 -tree can be found in Figure 2.

To be specific, we consider the K^2 -tree representation $(\mathcal{T}, \mathcal{X})$ of an adjacency matrix A as a K^2 -ary tree $\mathcal{T} = (\mathcal{V}, \mathcal{E})$ associated with binary node attributes $\mathcal{X} = \{x_u : u \in \mathcal{V}\}$. Every non-root node is uniquely indexed as (i, j) -th child of its parent node for some $i, j \in \{1, \dots, K\}$. The tree \mathcal{T} is

¹By default, we assume the number of nodes in the original graph to be the power of K^2 .

ordered so that every (i, j) -th child node is ranked $K(i - 1) + j$ among its siblings. Then the K^2 -tree satisfies the following conditions:

- Each tree-node u is associated with a submatrix $A^{(u)}$ of the adjacency matrix A .
- If the submatrix $A^{(u)}$ for a tree-node u is filled only with zeros, $x_u = 0$. Otherwise, $x_u = 1$.
- A tree-node u is a leaf node if and only if $x_u = 0$ or the matrix $A^{(u)}$ is a 1×1 matrix.
- Let $B_{1,1}, \dots, B_{K,K}$ denote the $K \times K$ partitioning of the matrix $A^{(u)}$ with i, j corresponding to row- and column-wise order, respectively. The child nodes $v_{1,1}, \dots, v_{K,K}$ of the tree-node u are associated with the submatrices $B_{1,1}, \dots, B_{K,K}$, respectively.

The generated K^2 -tree is a compact description of graph G as any non-leaf node u with $x_u = 0$ summarizes a large submatrix filled only with zeros. In the worst-case scenario, the size of the K^2 -tree is $MK^2(\log_{K^2}(N^2/M) + O(1))$ [31], where N and M denote the number of nodes and edges in the original graph, respectively. This constitutes a significant improvement over the N^2 size of the full adjacency matrix.

Additionally, the K^2 -tree is a hierarchical representation of the original graph, ensuring that (1) each node within the tree represents the connectivity between a specific set of nodes, and (2) nodes closer to the root correspond to a larger set of nodes. We emphasize that the tree-nodes are associated with submatrices overlapping with the diagonal of the original adjacency matrix when they indicate intra-connectivity within a group of nodes. In contrast, the remaining tree-nodes describe the inter-connectivity between two distinct sets of nodes.

We also describe the detailed algorithms for constructing a K^2 -tree from a given graph G and recovering a graph from the K^2 -tree in [Appendices A](#) and [B](#), respectively. It is crucial to note that the ordering of the nodes in the adjacency matrix influences the construction of the K^2 -tree. We empirically discover that Cuthill-McKee (C-M) ordering [34] provides the most compact K^2 -tree.² Our explanation is that the C-M ordering is specifically designed to align the non-zero elements of a matrix near its diagonal so that there is a higher chance of encountering large submatrices filled only with zeros, which can be efficiently summarized in the K^2 -tree representation.

We also remark that our description assumes the size of the original graph to be the power of K^2 . However, these assumptions can be alleviated by adding “dummy nodes” to increase the size of the original graph. This marginally affects the compression ratio since the dummy nodes form submatrices filled with zeros, which can be summarized into a single tree node in the K^2 -tree representation. We empirically verify this in [Table 4](#).

4 Hierarchical Graph Generation with K^2 -trees

In this section, we present our novel method, hierarchical graph generation with K^2 -trees (HGGT). At the heart of our method is exploitation of the hierarchical and compact structure of the K^2 -tree representation of a graph. Our key idea is the transformation of the K^2 -tree into a highly compressed sequence through a process involving pruning and tokenization. Subsequently, we employ a masked Transformer, enhanced with tree-based positional encodings, for the autoregressive generation of this compressed sequence.

4.1 Sequential K^2 -tree representation

Here, we propose an algorithm to flatten the K^2 -tree into a sequence, which is essential for the autoregressive generation of the K^2 -tree. In particular, we aim to design a sequential representation that is even more compact than the K^2 -tree to minimize the number of decisions required for the generation of the K^2 -tree. To this end, we propose (1) pruning K^2 -tree by removing redundant tree-nodes, (2) flattening the pruned K^2 -tree into a sequence, and (3) applying tokenization based on the K^2 -tree structure. We provide an illustration of the overall process in [Figure 3](#).

Pruning the K^2 -tree. To obtain the pruned K^2 -tree, we identify and eliminate redundant tree-nodes due to the symmetry of the adjacency matrix for undirected graphs. In particular, without loss of

²We provide the results in [Section 5.3](#).

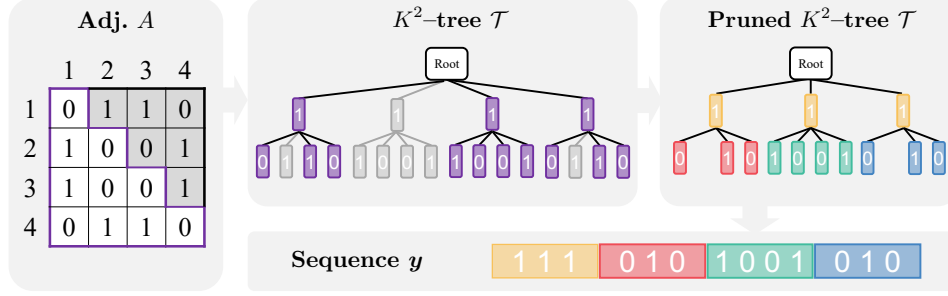


Figure 3: **Illustration of the sequential representation for K^2 -tree.** The shaded parts of the adjacency matrix A and the K^2 -tree \mathcal{T} denote redundant parts, which are further pruned, while the purple-colored parts of A and \mathcal{T} denote non-redundant parts. Also, same-colored tree-nodes of pruned K^2 -tree are grouped and tokenized into the same colored parts of the sequence y .

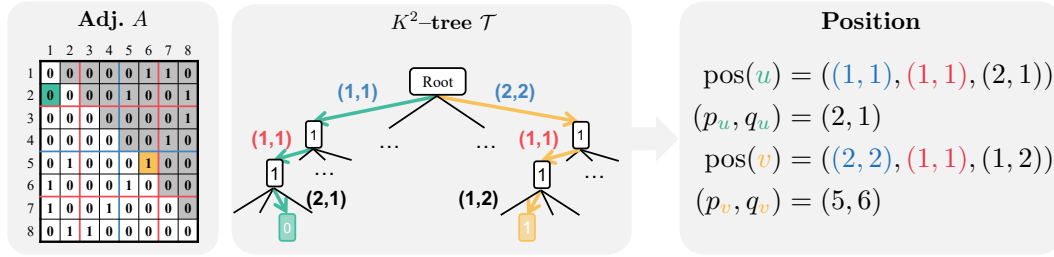


Figure 4: **Illustration of the tree-node positions of K^2 -tree.** The shaded parts of the adjacency matrix denote redundant parts, e.g., $p_u < q_u$. Additionally, colored elements correspond to tree-nodes of the same color and the same-colored tree-edges signify the root-to-target downward path. Blue and red tuples denote the order in the first and second levels, respectively. The tree node u is non-redundant as $p_u > q_u$ while v is redundant as $p_v < q_v$.

generality, such tree-nodes are associated with submatrices positioned above the diagonal since they mirror the counterparts located below the diagonal.

To this end, we now describe a formula to identify redundant tree-nodes by identifying the position of a submatrix $A^{(u)}$, tied to a specific tree-node u , within the adjacency matrix A . To this end, we consider a downward path v_0, v_1, \dots, v_L from the root node $r = v_0$ to the tree-node $u = v_L$ as description of the tree-node position. We also let (i_{v_ℓ}, j_{v_ℓ}) denote the order of v_ℓ among its siblings. Hence, the tree-node position can be represented as $\text{pos}(u) = ((i_{v_1}, j_{v_1}), \dots, (i_{v_L}, j_{v_L}))$. Also, the location of the submatrix $A^{(u)}$ is derived as the $(p_u, q_u) = (\sum_{\ell=1}^L K^{L-\ell}(i_{v_\ell} - 1) + 1, \sum_{\ell=1}^L K^{L-\ell}(j_{v_\ell} - 1) + 1)$ -th element with respect to the $K^L \times K^L$ partition of the adjacency matrix A , as described in Figure 4. As a result, we eliminate any tree-node associated with a submatrix above the diagonal, i.e., we remove tree-node u when $p_u < q_u$.

Consequently, the pruned K^2 -tree maintains only tree-nodes associated with submatrices devoid of redundant nodes, i.e., those containing elements of the adjacency matrix positioned at the diagonal or below the diagonal. Notably, following this pruning process, the K^2 -tree no longer adheres to the structure of a $K \times K$ -ary tree. Additionally, consider a non-leaf tree-node u is associated with a submatrix $A^{(u)}$ that includes any diagonal elements of the adjacency matrix A . Then the tree-node u will possess $K(K+1)/2$ child nodes, from the pruning of $K(K-1)/2$ child nodes previously associated with redundant submatrices. Otherwise, the non-leaf tree-node u will remain associated with $K \times K$ child nodes.

Flattening and tokenization of the pruned K^2 -tree. Next, we explain how to obtain a sequential representation of the pruned K^2 -tree based on flattening and tokenization. Our idea is to flatten a K^2 -tree as a sequence of tree-node attributes $\{x_u : u \in \mathcal{V}\}$ using breadth-first traversal and then to tokenize the sequence by grouping the tree-nodes that share the same parent node, i.e., sibling nodes.

For this purpose, we denote the sequence of tree-nodes obtained from a breadth-first traversal of non-root tree-nodes in the K^2 -tree as $u_1, \dots, u_{|\mathcal{V}|-1}$, and the corresponding sequence of node attributes

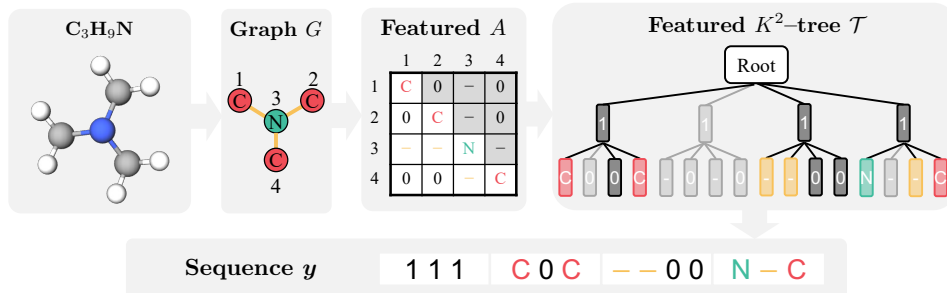


Figure 5: **An example of featured K^2 -tree representation.** The shaded parts of the adjacency matrix and K^2 -tree denote the redundant parts. The black-colored tree-nodes denote the normal tree-nodes with binary attributes while other-colored feature elements in the adjacency matrix A denote the same-colored featured tree-nodes and sequence elements. The node features (i.e., C and N) and edge feature (i.e., single bond $-$) of the molecule are represented within the leaf nodes.

as $x = (x_1, \dots, x_{|V|-1})$. It’s important to note that sibling nodes sharing the same parent appear sequentially in the breadth-first traversal.

Next, by grouping the sibling nodes, we tokenize the sequence x . As a result, we obtain a sequence $y = (y_1, \dots, y_T)$ where each element is a token representing a group of attributes associated with sibling nodes. For example, the t -th token corresponding to a group of K^2 sibling nodes is represented by $y_t = (x_{v_{1,1}}, \dots, x_{v_{K,K}})$ where $v_{1,1}, \dots, v_{K,K}$ share the same parent node u . Such tokenization allows representing the whole K^2 -tree using $M(\log_{K^2}(N^2/M) + O(1))$ space, where N and M denote the number of nodes and edges in the original graph, respectively.

We highlight that the number of elements in each token y_t may vary due to the pruned K^2 -tree no longer being a $K \times K$ -ary tree, as mentioned above. With this in consideration, we generate a vocabulary of $2^{K^2} + 2^{K(K+1)/2}$ potential configurations for each token y_t . This vocabulary size is small in practice since we set the value K to be small, e.g., setting $K = 2$ induces the size of 24.

In particular, we remark that a token with $K(K+1)/2$ elements carries different semantics from another token with K^2 elements. The former corresponds to a submatrix situated on the adjacency matrix’s diagonal, thus indicating connectivity *within* a set of nodes. In contrast, the latter relates to a submatrix illustrating connectivity *between* pairs of node sets. This supports our decision to assign distinct values to a token with $K(K+1)/2$ elements and another with K^2 elements, even when the tokens might represent the same combination of node features in the unpruned tree.

Generating featured graphs. We also extend our HGGT to graphs with node and edge-wise features, e.g., molecular graphs. At a high level, we apply our algorithm to the featured adjacency matrix, where each diagonal element corresponds to a node feature and each non-diagonal element corresponds to an edge feature. Tree-node attributes of leaf nodes in K^2 -tree correspond to node and edge features, while attributes of non-leaf nodes are the same with the non-attributed K^2 -trees (i.e., ones and zeros). See Figure 5 for an illustration and Appendix C for a complete description.

4.2 Generating K^2 -tree with Transformer and K^2 -tree positional encoding

Next, we describe our algorithm to generate the sequence of K^2 -tree representation $y = (y_1, \dots, y_T)$. We utilize the masked Transformer [19] to make predictions on $p_\theta(y_t|y_{t-1}, \dots, y_1)$. To improve the Transformer’s understanding of the tree structure, we devise a tree-positional encoding. We also offer an iterative algorithm to construct the K^2 -tree from the sequence generated by the Transformer.

Transformer with K^2 -tree positional encoding. We first propose the Transformer architecture to parameterize the distribution $p_\theta(y_t|y_{t-1}, \dots, y_1)$. To this end, we base our architecture on the Transformer architecture used for the autoregressive generation of sequential data. We use the tree-positional encodings for each time-step t to incorporate the structure of K^2 -tree during generation.

As outlined in Section 4.1, the node attributes in y_t are associated with child nodes of a particular tree-node u . To enhance the input y_t , we incorporate the positional encoding for u . This encoding is based on the downward path from the root node $r = v_0$ to the tree-node $u = v_L$, represented as (v_0, \dots, v_L) . In this context, the order of v_ℓ amongst its siblings in the non-pruned K^2 -tree is denoted as (i_{v_ℓ}, j_{v_ℓ}) .

Table 1: **Generic graph generation performance.** The baseline results are from prior works [8; 23; 35; 36] or obtained by running the open-source codes (marked by *). For each metric, the best number is highlighted in **bold** and the second-best number is underlined.

Method	Community-small			Planar			Enzymes			Grid		
	$12 \leq V \leq 20$			$ V = 64$			$10 \leq V \leq 125$			$100 \leq V \leq 400$		
	Deg.	Clus.	Orb.	Deg.	Clus.	Orb.	Deg.	Clus.	Orb.	Deg.	Clus.	Orb.
GraphVAE [5]	0.350	0.980	0.540	-	-	-	1.369	0.629	0.191	1.619	0.000	0.919
GraphRNN [18]	0.080	0.120	0.040	0.005	0.278	1.254	0.017	0.062	0.046	0.064	0.043	0.021
GNF [37]	0.200	0.200	0.110	-	-	-	-	-	-	-	-	-
GRAN [23]	-	-	-	<u>0.001</u>	0.043	<u>0.001</u>	-	-	-	<u>0.001</u>	<u>0.004</u>	<u>0.002</u>
EDP-GNN [24]	0.053	0.144	0.026	-	-	-	0.023	0.268	0.082	0.455	0.238	0.328
GraphGen [13]*	0.075	0.065	0.014	1.762	1.423	1.640	0.146	0.079	0.054	1.550	0.017	0.860
GraphAF [25]	0.180	0.200	0.020	-	-	-	1.669	1.283	0.266	-	-	-
GraphDF [26]	0.060	0.120	0.030	-	-	-	1.503	1.283	0.266	-	-	-
SPECTRE [35]	-	-	-	0.010	0.668	0.010	-	-	-	-	-	-
GDSS [8]	0.045	0.086	0.007	-	-	-	0.026	0.061	<u>0.009</u>	0.111	0.005	0.070
DiGress [9]*	0.012	0.025	<u>0.002</u>	0.000	<u>0.002</u>	0.008	<u>0.011</u>	<u>0.039</u>	0.010	0.016	0.000	0.004
GDSM [36]	<u>0.011</u>	<u>0.015</u>	0.001	-	-	-	0.013	0.088	0.010	0.002	0.000	0.000
HGGT (ours)	0.001	0.006	0.003	0.000	0.001	0.000	0.005	0.017	0.000	0.000	0.000	0.000

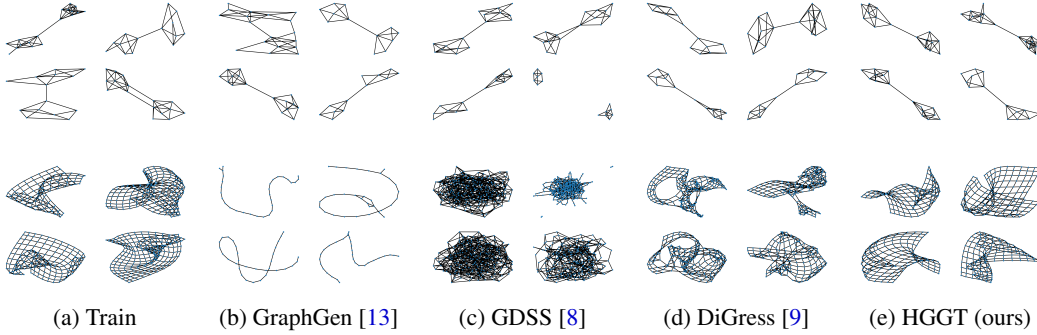


Figure 6: Generated samples for Community-small (top), and Grid (bottom) datasets.

Subsequently, we further update the input feature y_t through the addition of positional encoding, which is represented as $\text{PE}(u) = \sum_{\ell=1}^L \text{Embedding}_{\ell}(i_{v_{\ell}}, j_{v_{\ell}})$, where $((i_{v_1}, j_{v_1}), \dots, (i_{v_L}, j_{v_L}))$ are the sequence of orders of a downward path from the root node r to the tree-node u .

Constructing K^2 -tree from the sequential representation. We next explain the algorithm to recover a K^2 -tree from its sequential representation \mathbf{y} . In particular, we generate the K^2 -tree simultaneously with the sequence to incorporate the tree information for each step of the autoregressive generation. The algorithm begins with an empty tree containing only a root node and iteratively expands each “frontier” node based on the sequence of the decisions made by the generative model. To facilitate a breadth-first expansion approach, the algorithm utilizes a first-in-first-out (FIFO) queue, which contains tree-node candidates to be expanded.

To be specific, our algorithm initializes a K^2 -tree $\mathcal{T} = (\{r\}, \emptyset)$ with the root node r associated with the node attribute $x_r = 1$. It also initializes the FIFO queue \mathcal{Q} with the root node r . Then at each t -th iteration, our algorithm expands the tree-node u popped from the queue \mathcal{Q} using the token y_t . To be specific, for each tree-node attribute x in y_t , our algorithm adds a child node v with $x_v = x$. If $x = 1$ and the size of $A^{(v)}$ is larger than 1×1 , the child node v is inserted into the queue \mathcal{Q} . This algorithm is designed to retrieve the pruned tree, which allows for the computation of positional data derived from the y_t information.

5 Experiment

5.1 Generic graph generation

Experimental setup. We first validate the general graph generation performance of our HGGT on four synthetic and real graph datasets employed in previous works [35; 38]: (1) **Community-small**,

Table 2: **Molecular graph generation performance.** The baseline results are from prior works [8; 36] or obtained by running the open-source codes (denoted by *). The best results are highlighted in **bold** and the second best results are underlined.

Method	QM9					ZINC250k				
	Val. \uparrow	NSPDK \downarrow	FCD \downarrow	Uniq. \uparrow	Nov. \uparrow	Val. \uparrow	NSPDK \downarrow	FCD \downarrow	Uniq. \uparrow	Nov. \uparrow
EDP-GNN [24]	47.52	0.005	2.68	99.25	86.58	82.97	0.049	16.74	99.79	100
MoFlow [39]	91.36	0.017	4.47	<u>98.65</u>	94.72	63.11	0.046	20.93	99.99	100
GraphAF [25]	74.43	0.020	5.27	88.64	86.59	68.47	0.044	16.02	98.64	100
GraphDF [26]	93.88	0.064	10.93	98.58	98.54	90.61	0.177	33.55	99.63	100
GraphEBM [7]	8.22	0.030	6.14	97.90	97.01	5.29	0.212	35.47	98.79	100
GDSS [8]	95.72	0.003	2.9	98.46	86.27	<u>97.01</u>	<u>0.019</u>	<u>14.66</u>	99.64	100
DiGress [26]*	99.01	<u>0.001</u>	0.25	96.34	35.46	100	0.042	16.54	<u>99.97</u>	100
GDSM [36]	99.90	0.003	2.65	-	-	92.70	0.017	12.96	-	-
HGGT (ours)	<u>99.22</u>	0.000	<u>0.40</u>	95.65	24.01	92.87	0.001	1.93	<u>99.97</u>	<u>99.83</u>

100 synthetic community graphs with two communities, (2) **Planar**, 200 synthetic planar graphs, (3) **Enzymes** [20], 587 protein tertiary structure graphs, and (4) **Grid**, 100 synthetic 2D grid graphs. We adopt maximum mean discrepancy (MMD) as our evaluation metric to compare three graph property distributions between generated graphs and test graphs: degree, clustering coefficient, and 4-node-orbit counts. The detailed descriptions of our experimental setup are in [Appendix D](#).

Baselines. We compare our HGGT with twelve deep graph generative models: GraphVAE [5], GraphRNN [18], GNF [37], GRAN [23], EDP-GNN [24], GraphGen [13], GraphAF [25], GraphDF [26], SPECTRE [35], GDSS [8], DiGress [9], and GDSM [36]. We provide a detailed description of the implementations in [Appendix E](#).

Results. We provide experimental results are in [Table 1](#). We observe that our HGGT clearly outperforms all the baselines on all the datasets. This verifies our model’s ability to effectively capture the structural information of graphs. In particular, we observe how the performance of HGGT is extraordinary for Grid. We hypothesize that HGGT achieves high performance due to capturing the coarse-grained structure of grid graphs.

In [Figure 6](#), we also present examples of generated graphs to demonstrate the efficacy of our proposed algorithm, HGGT, in capturing the structural information of training graphs more accurately compared to existing graph generative models. Notably, for Community graphs, HGGT successfully generates well-connected community graphs, whereas the GDSS occasionally fails to generate interconnected edges between two communities. Moreover, for Grid graphs, HGGT consistently generates grid-structured data, while all other baselines failed. This supports the superior performance of our proposed HGGT in general graph generation. We provide more generated samples in [Appendix F](#).

5.2 Molecular graph generation

To show that HGGT is capable of generating featured adjacency matrices, we extend our evaluation to generate molecular graphs associated with atom-wise and bond-wise features. This ensures a comprehensive assessment of our method’s ability to generate feature-rich graph structures in domains such as chemistry and bioinformatics.

Experimental setup. We use two molecular datasets: QM9 [22] and ZINC250k [21]. Following the previous work [38], we evaluate 10,000 generated molecules using six metrics: (a) the ratio of valid molecules without correction (Val.), (b) neighborhood subgraph pairwise distance kernel (NSPDK), which captures the MMD with respect to the distribution of local subgraph patterns considering node features and edge features, (c) Frechet ChemNet Distance (FCD), which measures the distance between generated molecules and training molecules based on the activations of the penultimate layer of ChemNet [40], (d) the ratio of unique molecules (Uniq.), and (e) the ratio of novel molecules that did not appear in training molecules (Nov.). We use the same split with [8] for a fair comparison. We provide additional details for the experimental setup in [Appendix D](#).

Baselines. We compare HGGT with eight deep graph generative models: EDP-GNN [24], MoFlow [39], GraphAF [25], GraphDF [26], GraphEBM [7], GDSS[8], DiGress [9], and GDSM[36]. We provide a detailed description of implementation in [Appendix E](#).

Table 3: Ablation study for algorithmic components of HGGT.

Group	PE	Prune	Community-small			Planar			Enzymes		
			Degree	Cluster.	Orbit	Degree	Cluster.	Orbit	Degree	Cluster.	Orbit
✗	✗	✗	0.072	0.199	0.080	0.346	1.824	1.403	0.050	0.060	0.021
✓	✗	✗	0.009	0.105	0.001	<u>0.003</u>	0.001	<u>0.002</u>	<u>0.005</u>	0.022	0.007
✓	✓	✗	<u>0.002</u>	<u>0.028</u>	0.001	<u>0.003</u>	0.001	<u>0.002</u>	0.002	<u>0.020</u>	<u>0.002</u>
✓	✓	✓	0.001	0.006	<u>0.003</u>	0.000	0.001	0.000	<u>0.005</u>	0.017	0.000

Results. The experimental results are reported in Table 2. We observe that our HGGT showed competitive results on all the baselines on most of the metrics. This also confirms the effectiveness of our modification of HGGT to generate the featured graph. In particular, for the ZINC250k dataset, we observe a large gap between our method and the baselines for NSPKD and FCD scores. This verifies the ability of our model to be trained on large molecular graphs.

5.3 Ablation studies

We conduct three ablation studies to verify (1) the effectiveness of each component of sequential representation of K^2 -tree, (2) the necessity of proper choice of positional encoding, and (3) the effect of node orderings on the compression ratio.

Ablation of algorithmic components. We introduced three components to enhance the performance of HGGT: grouping into tokens (Group), incorporating tree positional encoding (PE), and pruning the K^2 -tree (Prune). To verify the effectiveness of each component, we present the experimental results for our method with incremental inclusion of these components. The experimental results are reported in Table 3. The results demonstrate the importance of each component in improving graph generation performance, with grouping being particularly crucial, thereby validating the significance of our additional components to the sequential K^2 -tree representation.

Positional encoding. In this experiment, we assess the impact of various positional encodings in our method. We compare our tree positional encoding (TPE) to absolute positional encoding (APE) and relative positional encoding (RPE). Our findings, as presented in Figure 7, demonstrate that TPE outperforms other positional encodings with faster convergence of training loss. These observations highlight the importance of an appropriate choice of positional encoding for generating high-quality graphs.

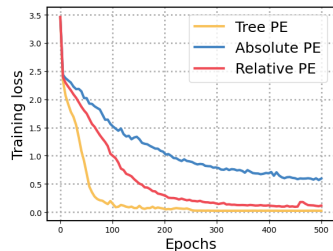


Figure 7: Training curve for different positional encodings on Planar.

Adjacency matrix orderings. It is clear that the choice of node order in the adjacency matrix A influences the size of K^2 -tree. We verify our design choice to use of Cuthill-McKee (C-M) ordering [34] by comparing its compression ratio to two other common node orderings: breadth-first search (BFS) and depth-first search (DFS). The compression ratio is defined as the number of elements in K^2 -tree divided by the number of cells in the adjacency matrix. In Table 4, we present the compression ratio results for each node ordering. Here, one can observe that C-M ordering shows the best compression ratio in most of the datasets compared to other orderings. Notably, K^2 -tree demonstrates a good compression rate even after adding dummy nodes to construct a proper K^2 -tree as claimed in Section 3.

Table 4: Average graph compression ratio for different matrix orderings on generic graphs.

Method	Comm.	Planar	Enzymes	Grid
BFS	0.534	0.201	0.432	0.048
DFS	0.619	0.204	0.523	0.064
C-M	0.508	0.195	0.404	0.045

6 Conclusion

In this paper, we presented a novel K^2 -tree-based graph generation representation (HGGT) for generating graphs in a compact, hierarchical, and domain-agnostic manner. Our experimental evaluation demonstrated that the proposed HGGT achieves state-of-the-art performance across

various graph datasets, including synthetic, real-world, and molecular graphs. An interesting avenue for future work is that the broader examination of other graph representations to graph generation (e.g., a plethora of representations [41; 42]) exists even when just considering the domain of lossless graph compression. We also consider generating our K^2 -tree representation with different architectures, e.g., using diffusion models to sequentially generate each level of the K^2 -tree, to be a solid and interesting future work.

References

- [1] Yujia Li, Oriol Vinyals, Chris Dyer, Razvan Pascanu, and Peter Battaglia. Learning deep generative models of graphs. *arXiv preprint arXiv:1803.03324*, 2018. 1
- [2] Łukasz Maziarka, Agnieszka Pocha, Jan Kaczmarczyk, Krzysztof Rataj, Tomasz Danel, and Michał Warchoń. Mol-cycleGAN: a generative model for molecular optimization. *Journal of Cheminformatics*, 12(1):1–18, 2020. 1
- [3] Aditya Grover, Aaron Zweig, and Stefano Ermon. Graphite: Iterative generative modeling of graphs. In *International conference on machine learning*, pages 2434–2444. PMLR, 2019. 1
- [4] Hao Yu, Xu Sun, Wei Deng Solvang, and Xu Zhao. Reverse logistics network design for effective management of medical waste in epidemic outbreaks: Insights from the coronavirus disease 2019 (covid-19) outbreak in wuhan (china). *International journal of environmental research and public health*, 17(5):1770, 2020. 1
- [5] Martin Simonovsky and Nikos Komodakis. Graphvae: Towards generation of small graphs using variational autoencoders. In *Artificial Neural Networks and Machine Learning–ICANN 2018: 27th International Conference on Artificial Neural Networks, Rhodes, Greece, October 4–7, 2018, Proceedings, Part I* 27, pages 412–422. Springer, 2018. 1, 3, 7, 8, 18
- [6] Kaushalya Madhawa, Katushiko Ishiguro, Kosuke Nakago, and Motoki Abe. Graphnvp: An invertible flow model for generating molecular graphs. *arXiv preprint arXiv:1905.11600*, 2019. 1
- [7] Meng Liu, Keqiang Yan, Bora Oztekin, and Shuiwang Ji. Graphebm: Molecular graph generation with energy-based models. *arXiv preprint arXiv:2102.00546*, 2021. 1, 8, 18
- [8] Jaehyeong Jo, Seul Lee, and Sung Ju Hwang. Score-based generative modeling of graphs via the system of stochastic differential equations. In *International Conference on Machine Learning*, pages 10362–10383. PMLR, 2022. 1, 2, 3, 7, 8, 17, 18
- [9] Clement Vignac, Igor Krawczuk, Antoine Siraudin, Bohan Wang, Volkan Cevher, and Pascal Frossard. Digress: Discrete denoising diffusion for graph generation. *arXiv preprint arXiv:2209.14734*, 2022. 1, 3, 7, 8, 18
- [10] Réka Albert and Albert-László Barabási. Statistical mechanics of complex networks. *Reviews of modern physics*, 74(1):47, 2002. 1
- [11] Paul Erdős, Alfréd Rényi, et al. On the evolution of random graphs. *Publ. Math. Inst. Hung. Acad. Sci.*, 5(1):17–60, 1960. 1
- [12] Sungsoo Ahn, Binghong Chen, Tianzhe Wang, and Le Song. Spanning tree-based graph generation for molecules. In *International Conference on Learning Representations*, 2022. URL https://openreview.net/forum?id=w60btE_8T2m. 1, 3
- [13] Nikhil Goyal, Harsh Vardhan Jain, and Sayan Ranu. Graphgen: a scalable approach to domain-agnostic labeled graph generation. In *Proceedings of The Web Conference 2020*, pages 1253–1263, 2020. 1, 2, 3, 7, 8, 18
- [14] Mario Krenn, Florian Häse, A Nigam, Pascal Friederich, and Alán Aspuru-Guzik. SELFIES: a robust representation of semantically constrained graphs with an example application in chemistry. *arXiv preprint arXiv:1905.13741*, 2019. 1, 3

- [15] Marwin HS Segler, Thierry Kogej, Christian Tyrchan, and Mark P Waller. Generating focused molecule libraries for drug discovery with recurrent neural networks. *ACS central science*, 4(1): 120–131, 2018. [1](#), [3](#)
- [16] Wengong Jin, Regina Barzilay, and Tommi Jaakkola. Junction tree variational autoencoder for molecular graph generation. In *International conference on machine learning*, pages 2323–2332. PMLR, 2018. [1](#), [2](#), [3](#)
- [17] Wengong Jin, Regina Barzilay, and Tommi Jaakkola. Hierarchical generation of molecular graphs using structural motifs. In *International conference on machine learning*, pages 4839–4848. PMLR, 2020. [1](#), [3](#)
- [18] Jiaxuan You, Rex Ying, Xiang Ren, William Hamilton, and Jure Leskovec. Graphrnn: Generating realistic graphs with deep auto-regressive models. In *International conference on machine learning*, pages 5708–5717. PMLR, 2018. [2](#), [3](#), [7](#), [8](#), [18](#)
- [19] Ashish Vaswani, Noam Shazeer, Niki Parmar, Jakob Uszkoreit, Llion Jones, Aidan N Gomez, Łukasz Kaiser, and Illia Polosukhin. Attention is all you need. *Advances in neural information processing systems*, 30, 2017. [2](#), [6](#), [18](#)
- [20] Ida Schomburg, Antje Chang, Christian Ebeling, Marion Gremse, Christian Heldt, Gregor Huhn, and Dietmar Schomburg. Brenda, the enzyme database: updates and major new developments. *Nucleic acids research*, 32(suppl_1):D431–D433, 2004. [2](#), [8](#)
- [21] John J Irwin, Teague Sterling, Michael M Mysinger, Erin S Bolstad, and Ryan G Coleman. Zinc: a free tool to discover chemistry for biology. *Journal of chemical information and modeling*, 52(7):1757–1768, 2012. [2](#), [8](#)
- [22] Raghunathan Ramakrishnan, Pavlo O Dral, Matthias Rupp, and O Anatole Von Lilienfeld. Quantum chemistry structures and properties of 134 kilo molecules. *Scientific data*, 1(1):1–7, 2014. [2](#), [8](#)
- [23] Renjie Liao, Yujia Li, Yang Song, Shenlong Wang, Will Hamilton, David K Duvenaud, Raquel Urtasun, and Richard Zemel. Efficient graph generation with graph recurrent attention networks. *Advances in neural information processing systems*, 32, 2019. [3](#), [7](#), [8](#), [18](#)
- [24] Chenhao Niu, Yang Song, Jiaming Song, Shengjia Zhao, Aditya Grover, and Stefano Ermon. Permutation invariant graph generation via score-based generative modeling. In *International Conference on Artificial Intelligence and Statistics*, pages 4474–4484. PMLR, 2020. [3](#), [7](#), [8](#), [18](#)
- [25] Chence Shi, Minkai Xu, Zhaocheng Zhu, Weinan Zhang, Ming Zhang, and Jian Tang. Graphaf: a flow-based autoregressive model for molecular graph generation. *arXiv preprint arXiv:2001.09382*, 2020. [3](#), [7](#), [8](#), [18](#)
- [26] Youzhi Luo, Keqiang Yan, and Shuiwang Ji. Graphdf: A discrete flow model for molecular graph generation. In *International Conference on Machine Learning*, pages 7192–7203. PMLR, 2021. [3](#), [7](#), [8](#), [18](#)
- [27] David Weininger. Smiles, a chemical language and information system. 1. introduction to methodology and encoding rules. *Journal of chemical information and computer sciences*, 28(1):31–36, 1988. [3](#)
- [28] Soojung Yang, Doyeong Hwang, Seul Lee, Seongok Ryu, and Sung Ju Hwang. Hit and lead discovery with explorative rl and fragment-based molecule generation. *Advances in Neural Information Processing Systems*, 34:7924–7936, 2021. [3](#)
- [29] Minghao Guo, Veronika Thost, Beichen Li, Payel Das, Jie Chen, and Wojciech Matusik. Data-efficient graph grammar learning for molecular generation. *arXiv preprint arXiv:2203.08031*, 2022. [3](#)
- [30] Maciej Besta and Torsten Hoeffler. Survey and taxonomy of lossless graph compression and space-efficient graph representations. *arXiv preprint arXiv:1806.01799*, 2018. [3](#)

- [31] Nieves R Brisaboa, Susana Ladra, and Gonzalo Navarro. k2-trees for compact web graph representation. In *SPIRE*, volume 9, pages 18–30. Springer, 2009. 3, 4
- [32] Sriram Raghavan and Hector Garcia-Molina. Representing web graphs. In *Proceedings 19th International Conference on Data Engineering (Cat. No. 03CH37405)*, pages 405–416. IEEE, 2003. 3
- [33] Giorgos Bouritsas, Andreas Loukas, Nikolaos Karalias, and Michael Bronstein. Partition and code: learning how to compress graphs. *Advances in Neural Information Processing Systems*, 34:18603–18619, 2021. 3
- [34] Elizabeth Cuthill and James McKee. Reducing the bandwidth of sparse symmetric matrices. In *Proceedings of the 1969 24th national conference*, pages 157–172, 1969. 4, 9
- [35] Karolis Martinkus, Andreas Loukas, Nathanaël Perraudin, and Roger Wattenhofer. Spectre: Spectral conditioning helps to overcome the expressivity limits of one-shot graph generators. In *International Conference on Machine Learning*, pages 15159–15179. PMLR, 2022. 7, 8, 18
- [36] Tianze Luo, Zhanfeng Mo, and Sinno Jialin Pan. Fast graph generative model via spectral diffusion. *arXiv preprint arXiv:2211.08892*, 2022. 7, 8, 17, 18
- [37] Jenny Liu, Aviral Kumar, Jimmy Ba, Jamie Kiros, and Kevin Swersky. Graph normalizing flows. *Advances in Neural Information Processing Systems*, 32, 2019. 7, 8, 18
- [38] Lingkai Kong, Jiaming Cui, Haotian Sun, Yuchen Zhuang, B. Aditya Prakash, and Chao Zhang. Autoregressive diffusion model for graph generation, 2023. URL <https://openreview.net/forum?id=98J48HZXd5>. 7, 8
- [39] Chengxi Zang and Fei Wang. Moflow: an invertible flow model for generating molecular graphs. In *Proceedings of the 26th ACM SIGKDD International Conference on Knowledge Discovery & Data Mining*, pages 617–626, 2020. 8, 18
- [40] Kristina Preuer, Philipp Renz, Thomas Unterthiner, Sepp Hochreiter, and Gunter Klambauer. Fréchet chemnet distance: a metric for generative models for molecules in drug discovery. *Journal of chemical information and modeling*, 58(9):1736–1741, 2018. 8
- [41] Paolo Boldi, Massimo Santini, and Sebastiano Vigna. Permuting web and social graphs. *Internet Mathematics*, 6(3):257–283, 2009. 10
- [42] N Jesper Larsson and Alistair Moffat. Off-line dictionary-based compression. *Proceedings of the IEEE*, 88(11):1722–1732, 2000. 10
- [43] Adam Paszke, Sam Gross, Francisco Massa, Adam Lerer, James Bradbury, Gregory Chanan, Trevor Killeen, Zeming Lin, Natalia Gimelshein, Luca Antiga, et al. Pytorch: An imperative style, high-performance deep learning library. *Advances in neural information processing systems*, 32, 2019. 18

A Construction of a K^2 -tree from the graph

Algorithm 1 K^2 -tree construction

Input: Adjacency matrix A and partitioning factor K .

- 1: Initialize the tree $\mathcal{T} \leftarrow (\mathcal{V}, \mathcal{E})$ with $\mathcal{V} = \emptyset, \mathcal{E} = \emptyset$. ▷ K^2 -tree.
- 2: Initialize an empty queue Q . ▷ Candidates to be expanded into child nodes.
- 3: Set $\mathcal{V} \leftarrow \mathcal{V} \cup \{r\}, x_r \leftarrow 1$ and let $A^{(r)} \leftarrow A$. Insert r into the queue Q . ▷ Add root node r .
- 4: **while** $Q \neq \emptyset$ **do**
- 5: Pop u from Q .
- 6: **if** $x_u = 0$ **then** ▷ Condition for not expanding the node u .
- 7: Go to line 4.
- 8: **end if**
- 9: Update $s \leftarrow \dim(A^{(u)})/K$
- 10: **for** $i = 1, \dots, K$ **do** ▷ Row-wise indices.
- 11: **for** $j = 1, \dots, K$ **do** ▷ Column-wise indices.
- 12: Set $B_{i,j} \leftarrow A^{(u)}[(i-1)s : is, (j-1)s : js]$.
▷ Operation to obtain $s \times s$ submatrix $B_{i,j}$ of $A^{(u)}$.
- 13: If $B_{i,j}$ is filled with zeros, set $x_v \leftarrow 1$. Otherwise, set $x_v \leftarrow 0$.
▷ Update tree-node attribute.
- 14: If $\dim(v_{i,j}) > 1$, update $Q \leftarrow v_{i,j}$.
- 15: **end for**
- 16: **end for**
- 17: Set $\mathcal{V} \leftarrow \mathcal{V} \cup \{v_{1,1}, \dots, v_{K,K}\}$. ▷ Update tree nodes.
- 18: Set $\mathcal{E} \leftarrow \mathcal{E} \cup \{(u, v_{1,1}), \dots, (u, v_{K,K})\}$. ▷ Update tree edges.
- 19: **end while**

Output: K^2 -tree $(\mathcal{T}, \mathcal{X})$ where $\mathcal{X} = \{x_u : u \in \mathcal{V}\}$.

In this section, we explain our algorithm to construct a K^2 -tree $(\mathcal{T}, \mathcal{X})$ from a given graph $G = A$ where G is a symmetric non-featured graph and A is an adjacency matrix. Note that the K^2 -ary tree $\mathcal{T} = (\mathcal{V}, \mathcal{E})$ is associated with binary node attributes $\mathcal{X} = \{x_u : u \in \mathcal{V}\}$. In addition, let $\dim(A)$ to denote the number of rows (or columns) n of the square matrix $A \in \{0, 1\}^{n \times n}$. We describe the full procedure in Algorithm 1.

B Constructing a graph from the K^2 -tree

Algorithm 2 Graph G construction

Input: K^2 -tree $(\mathcal{T}, \mathcal{X})$ and partitioning factor K .
Set $m \leftarrow K^{D_{\mathcal{T}}}$. ▷ Full adjacency matrix size.
Initialize $A \in \{0, 1\}^{m \times m}$ with zeros.
for $u \in \mathcal{L}$ **do** ▷ For each leaf node with $x_u = 1$.
 $\text{pos}(u) = ((i_{v_1}, j_{v_1}), \dots, (i_{v_L}, j_{v_L}))$. ▷ Position of node u .
 $(p_u, q_u) = (\sum_{\ell=1}^L K^{L-\ell}(i_{v_\ell} - 1) + 1, \sum_{\ell=1}^L K^{L-\ell}(j_{v_\ell} - 1) + 1)$. ▷ Location of node u .
 Set $A_{p_u, q_u} \leftarrow 1$.
end for
Output: Adjacency matrix A .

We next describe the algorithm to generate a graph $G = A$ given the K^2 -tree $(\mathcal{T}, \mathcal{X})$ with tree depth $D_{\mathcal{T}}$. Let $\mathcal{L} \subset \mathcal{V}$ be the set of leaf nodes in K^2 -tree with node attributes 1. Note that we represent the tree-node position of $u \in \mathcal{V}$ as $\text{pos}(u) = ((i_{v_1}, j_{v_1}), \dots, (i_{v_L}, j_{v_L}))$ based on a downward path v_0, v_1, \dots, v_L from the root node $r = v_0$ to the tree-node $u = v_L$. In addition, the location of corresponding submatrix $A^{(u)}$ is denoted as $(p_u, q_u) = (\sum_{\ell=1}^L K^{L-\ell}(i_{v_\ell} - 1) + 1, \sum_{\ell=1}^L K^{L-\ell}(j_{v_\ell} - 1) + 1)$ in as described in [Section 4.1](#). We describe the full procedure as in [Algorithm 2](#).

C Generalizing K^2 -tree to Attributed Graphs

Algorithm 3 Featured K^2 -tree construction

Input: Modified adjacency matrix A and partitioning factor K .

- 1: Initialize the tree $\mathcal{T} \leftarrow (\mathcal{V}, \mathcal{E})$ with $\mathcal{V} = \emptyset, \mathcal{E} = \emptyset$. ▷ Featured K^2 -tree.
- 2: Initialize an empty queue Q . ▷ Candidates to be expanded into child nodes.
- 3: Set $\mathcal{V} \leftarrow \mathcal{V} \cup \{r\}, x_r \leftarrow 1$ and let $A^{(r)} \leftarrow A$. Insert r into the queue Q . ▷ Add root node r .
- 4: **while** $Q \neq \emptyset$ **do**
- 5: Pop u from Q .
- 6: **if** $x_u = 0$ **then** ▷ Condition for not expanding the node u .
- 7: Go to line 4.
- 8: **end if**
- 9: Update $s \leftarrow \dim(A^{(u)})/K$
- 10: **for** $i = 1, \dots, K$ **do** ▷ Row-wise indices.
- 11: **for** $j = 1, \dots, K$ **do** ▷ Column-wise indices.
- 12: Set $B_{i,j} \leftarrow A^{(u)}[(i-1)s : is, (j-1)s : js]$. ▷ Operation to obtain $s \times s$ submatrix $B_{i,j}$ of $A^{(u)}$.
- 13: **if** $B_{i,j}$ is filled with zeros **then** ▷ Update tree-node attribute.
- 14: Set $x_v \leftarrow 0$.
- 15: **else if** $|B_{i,j}| > 1$ **then** ▷ Non-leaf tree-nodes with attribute 1.
- 16: Set $x_v \leftarrow 1$.
- 17: **else** ▷ Leaf tree-nodes with node features and edge features.
- 18: Set $x_v \leftarrow B_{i,j}$. ▷ We treat 1×1 matrix $B_{i,j}$ as a scalar.
- 19: **end if**
- 20: **if** $\dim(B_{i,j}) > 1$ **then** $Q \leftarrow v_{i,j}$.
- 21: **end if**
- 22: **end for**
- 23: **end for**
- 24: Set $\mathcal{V} \leftarrow \mathcal{V} \cup \{v_{1,1}, \dots, v_{K,K}\}$. ▷ Update tree nodes.
- 25: Set $\mathcal{E} \leftarrow \mathcal{E} \cup \{(u, v_{1,1}), \dots, (u, v_{K,K})\}$. ▷ Update tree edges.
- 26: **end while**

Output: Featured K^2 -tree $(\mathcal{T}, \mathcal{X})$ where $\mathcal{X} = \{x_u : u \in \mathcal{V}\}$.

Algorithm 4 Featured graph G construction

- 1: **Input:** Featured K^2 -tree $(\mathcal{T}, \mathcal{X})$ and partitioning factor K .
- 2: $m \leftarrow K^{D\tau}$ ▷ Full adjacency matrix size.
- 3: Initialize $A \in \{0, 1\}^{m \times m}$ with zeros.
- 4: **for** $u \in \mathcal{L}$ **do** ▷ For each leaf node with $x_u \neq 0$.
- 5: $\text{pos}(u) = ((i_{v_1}, j_{v_1}), \dots, (i_{v_L}, j_{v_L}))$. ▷ Position of node u .
- 6: $(p_u, q_u) = (\sum_{\ell=1}^L K^{L-\ell}(i_{v_\ell} - 1) + 1, \sum_{\ell=1}^L K^{L-\ell}(j_{v_\ell} - 1) + 1)$. ▷ Location of node u .
- 7: Set $A_{p_u, q_u} \leftarrow x_u$.
- 8: **end for**
- 9: **Output:** Modified adjacency matrix A .

In this section, we describe a detailed process to construct a K^2 -tree for featured graphs with node features and edge features (e.g., molecular graphs), which is described briefly in [Section 4.1](#). We modify the original adjacency matrix by incorporating categorical features into each element, thereby enabling the derivation of the featured K^2 -tree from the modified adjacency matrix.

Edge features. Integrating edge features into the adjacency matrix is straightforward. It can be accomplished by simply replacing the ones with the appropriate categorical edge features.

Node features. Integrating node features into the adjacency matrix is more complex than that of edge features since the adjacency matrix only describes the connectivity between node pairs. To address this issue, we assume that all graph nodes possess self-loops, which leads to filling ones to the diagonal elements. Then we replace ones on the diagonal with categorical node features that correspond to the respective node positions.

Let $x_u \in \mathcal{X}$ be the non-binary tree-node attributes that include node features and edge features and \mathcal{L} be the set of leaf nodes in K^2 -tree with non-zero node attributes. Then we can construct a featured K^2 -tree with a modified adjacency matrix and construct a graph G from the featured K^2 -tree as described in [Algorithm 3](#) and [Algorithm 4](#), respectively.

D Experimental Details

In this section, we provide the details of the experiments. Note that we chose $k = 2$ in all experiments and provide additional experimental results for $k = 3$ in [Appendix G](#).

D.1 Generic graph generation

Table 5: **Hyperparameters of HGGT in generic graph generation.**

	Hyperparameters	Community-small	Planar	Enzymes	Grid
Transformer	Dim. of feedforward network	512	512	512	512
	Transformer dropout rate	0.1	0	0.1	0.1
	Nu of attention heads	8	8	8	8
	# of layers	3	3	3	3
Train	Batch size	128	32	32	8
	# of epochs	500	500	500	500
	Dim. of token embedding	512	512	512	512
	Gradient clipping norm	1	1	1	1
	Input dropout rate	0	0	0	0
	Learning rate	1×10^{-3}	1×10^{-3}	2×10^{-4}	5×10^{-4}

We used the same split with GDSS [8] for Community-small, Enzymes, and Grid datasets. Otherwise, we used the same split with SPECTRE [36] for the Planar dataset. We fix $k = 2$ and perform the hyperparameter search to choose the best learning rate in $\{0.0001, 0.0002, 0.0005, 0.001\}$ and the best dropout rate in $\{0, 0.1\}$. We select the model with the best MMD with the lowest average of three graph statistics: degree, clustering coefficient, and orbit count. Finally, we provide the hyperparameters used in the experiment in [Table 7](#).

D.2 Molecular graph generation

Table 6: **Statistics of molecular datasets: QM9 and ZINC250k.**

Dataset	# of graphs	# of nodes	# of node types	# of edge types
QM9	133,885	$1 \leq V \leq 9$	4	3
ZINC250k	249,455	$6 \leq V \leq 38$	9	3

Table 7: **Hyperparameters of HGGT in molecular graph generation.**

	Hyperparameter	QM9	ZINC250k
Transformer	Dim. of feedforward network	512	512
	Transformer dropout rate	0.1	0.1
	# of attention heads	8	8
	# of layers	2	3
Train	Batch size	1024	256
	# of epochs	500	500
	Dim. of token embedding	512	512
	Gradient clipping norm	1	1
	Input dropout rate	0.5	0
	Learning rate	5×10^{-4}	5×10^{-4}

The statistics of training molecular graphs (i.e., QM9 and ZINC250k datasets) are summarized in [Table 6](#) and we used the same split with GDSS [8] for a fair evaluation. We fix $k = 2$ and perform the hyperparameter search to choose the best number of layers in $\{2, 3\}$ and select the model with the best validity. In addition, we provide the hyperparameters used in the experiment in [Table 7](#).

E Implementation Details

E.1 Computing resources

We used PyTorch [43] to implement HGGT and train the Transformer [19] models on GeForce RTX 3090 GPU.

E.2 Model architecture

We describe the architecture of the proposed transformer generator of HGGT in Figure 8. The generator takes a sequential representation of K^2 -tree as input and generates the output probability of each token as described in Section 4.2. The model consists of a token embedding layer, transformer encoder(s), and multilayer perceptron layer with tree positional encoding.

E.3 Details for baseline implementation

Generic graph generation. The baseline results from prior works are as follows. Results for GraphVAE [5], GraphRNN [18], GNF [37], EDP-GNN [24], GraphAF [25], GraphDF [26], and GDSS [8] are obtained from GDSS, while the results for GRAN [23], SPECTRE [35], and GDSM [36] are derived from their respective paper. Additionally, we reproduced DiGress [9] and GraphGen [13] using their open-source codes. We used original hyperparameters when the original work provided them. DiGress takes more than three days for the Planar, Enzymes, and Grid datasets, so we report the results from fewer epochs after convergence.

Molecular graph generation. The baseline results from prior works are as follows. The results for EDP-GNN [24], MoFlow [39], GraphAF [25], GraphDF [26], GraphEBM [7], and GDSS [8] are from GDSS, and the GDSM [36] result is extracted from the corresponding paper. Moreover, we reproduced DiGress [9] using their open-source codes.

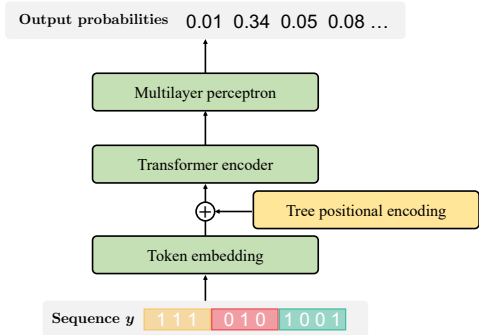


Figure 8: The architecture of the transformer generator of HGGT.

F Generated samples

In this section, we provide the visualizations of the generated graphs for generic and molecular graph generation.

F.1 Generic graph generation

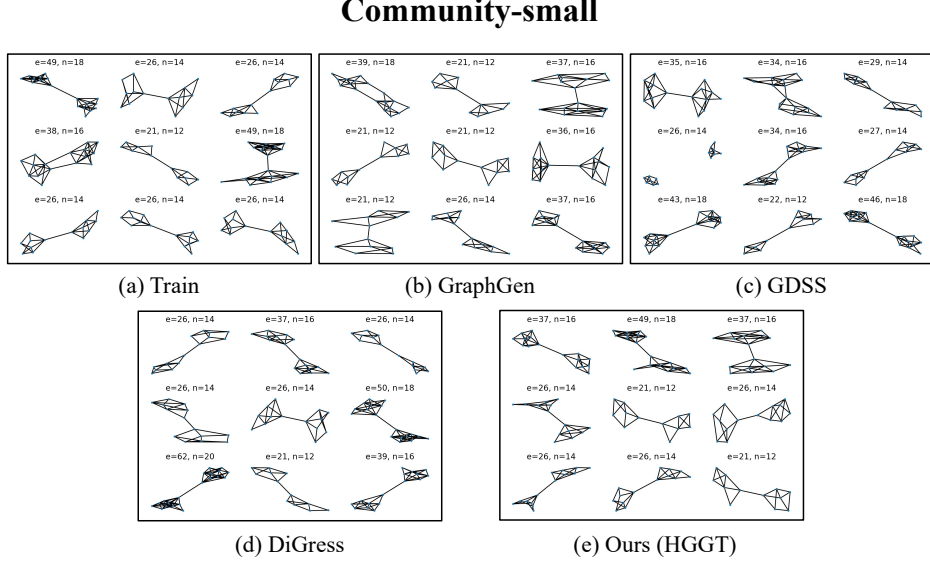


Figure 9: Visualization of the graphs from the Community-small dataset and the generated graphs.

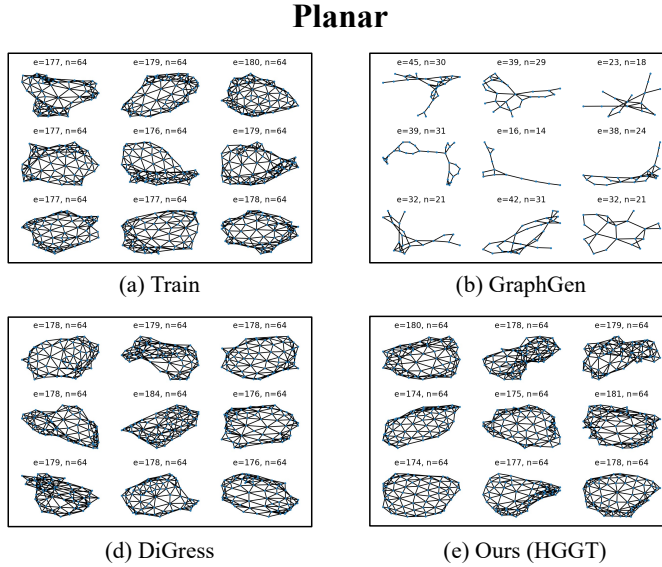


Figure 10: Visualization of the graphs from the Planar dataset and the generated graphs.

We present visualizations of graphs from the training dataset and generated samples from GraphGen, DiGress, GDSS, and HGGT in Figure 9, Figure 10, Figure 11, and Figure 12. Note that we reproduced GraphGen and DiGress using open-source codes while utilizing the provided checkpoints for GDSS. However, given that the checkpoints provided for GDSS do not include the Planar dataset, we have omitted GDSS samples for this dataset. We additionally give the number of nodes and edges of each graph.

Enzymes

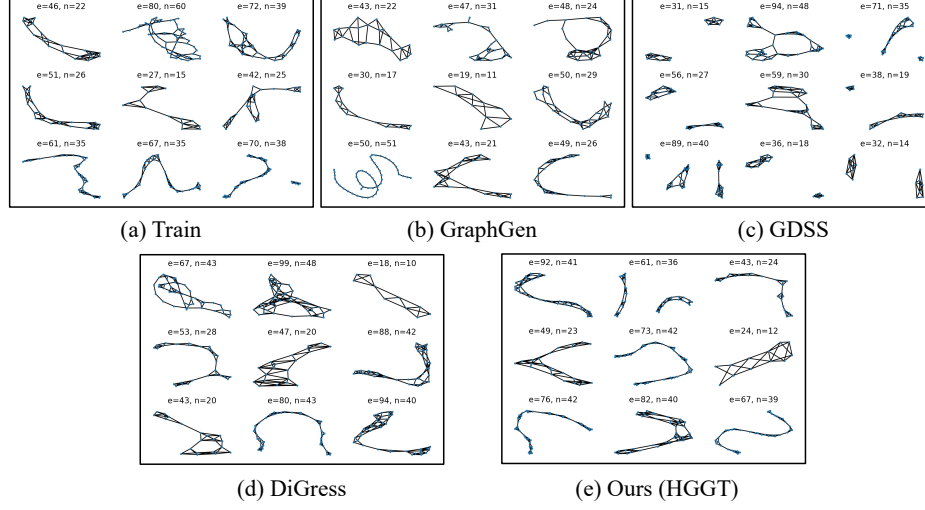


Figure 11: Visualization of the graphs from the enzymes dataset and the generated graphs.

Grid

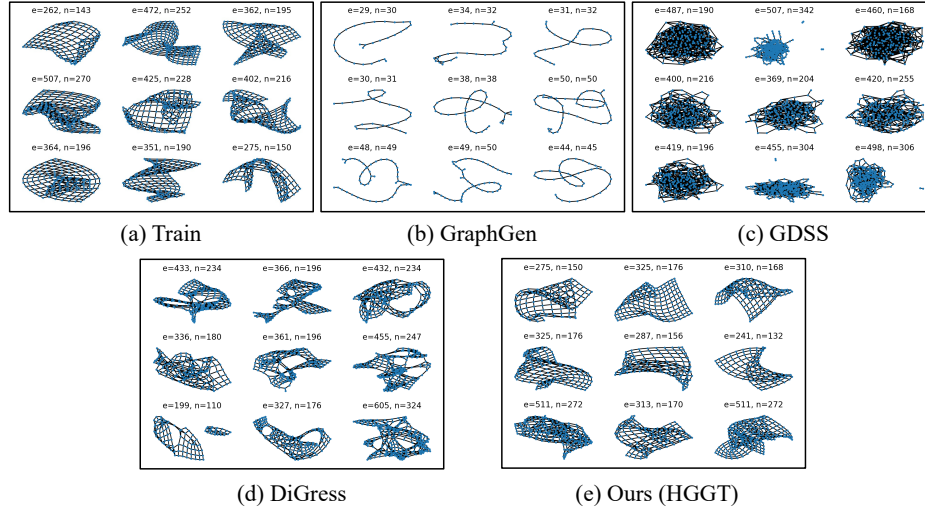


Figure 12: Visualization of the graphs from the Grid dataset and the generated graphs.

E.2 Molecular graph generation

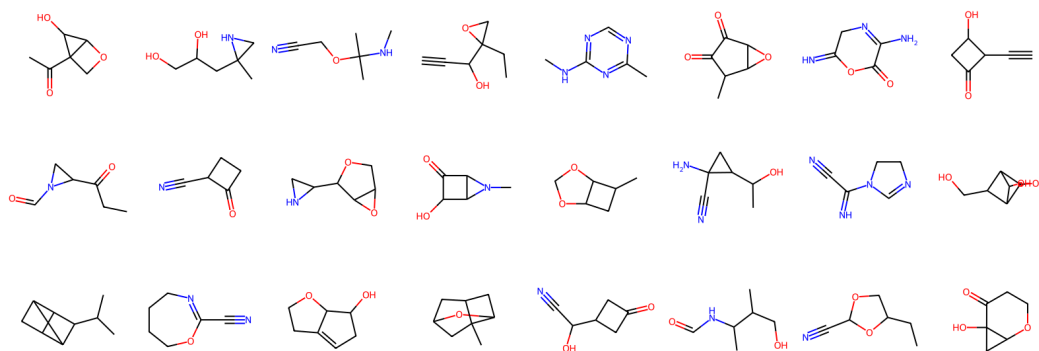


Figure 13: Visualization of the molecules generated from the QM9 dataset.

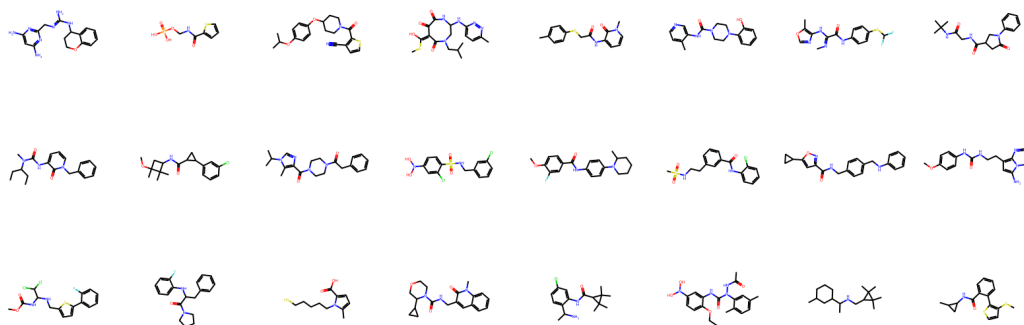


Figure 14: Visualization of the molecules generated from the ZINC250k dataset.

We present visualizations of generated molecules from HGGT in [Figure 13](#) and [Figure 14](#). Note that the 24 molecules are non-cherry-picked and randomly sampled.

G Additional Experimental Results

In this section, we report additional experimental results.

G.1 Generic graph generation

We provide generic graph generation results for $k = 3$. Increasing k decreases the sequence length, while vocabulary size increases to $2^{3^2} + 2^6 = 578$.

We used Community-small and Planar datasets and measured MMD between the test graphs and generated graphs. We perform the same hyperparameter search for a fair evaluation as $k = 2$. The results are in Table 8. We can observe that HGGT still outperforms the baselines even with different k .

Table 8: **Generation results of HGGT with $k = 3$.**

	Community-small			Planar		
	Degree	Cluster.	Orbit	Degree	Cluster.	Orbit
$k = 2$	0.001	0.006	0.003	0.000	0.001	0.000
$k = 3$	0.007	0.050	0.001	0.001	0.003	0.000

G.2 Molecular graph generation

Table 9: **Additional molecular graph generation performance.**

Method	QM9						
	Frag. \uparrow	Intdiv. \uparrow	QED \downarrow	SA \downarrow	SNN \uparrow	Scaf. \uparrow	Weight \downarrow
DiGress	0.9737	0.9189	0.0015	0.0189	0.5216	0.9063	0.1746
HGGT (Ours)	0.9874	0.9150	0.0012	0.0304	0.5156	0.9368	0.2430

Method	ZINC250k						
	Frag. \uparrow	Intdiv. \uparrow	QED \downarrow	SA \downarrow	SNN \uparrow	Scaf. \uparrow	Weight \downarrow
DiGress	0.7702	0.9061	0.1284	1.9290	0.2491	0.0001	62.9923
HGGT (Ours)	0.9877	0.8644	0.0164	0.2407	0.4383	0.5298	1.8592

We additionally report seven metrics of the generated molecules: (a) fragment similarity (Frag.), which measures the BRICS fragment frequency similarity between generated molecules and test molecules, (b) internal diversity (Intdiv.), which measures the chemical diversity in generated molecules, (c) quantitative estimation of drug-likeness (QED), which measures the drug-likeness similarity between generated molecules and test molecules, (d) synthetic accessibility score (SA), which compares the synthetic accessibility between generated molecules and test molecules, (e) similarity to the nearest neighbor (SNN), an average of Tanimoto similarity between the fingerprint of a generated molecule and test molecule, (f) scaffold similarity (Scaf.), the Bemis-Murcko scaffold frequency similarity between generated molecules and test molecules, and (g) weight, the atom weight similarity between generated molecules and test molecules. The results are in Table 9.